HEFAT2014
10th International Conference on Heat Transfer, Fluid Mechanics and Thermodynamics
14 – 16 July 2014
Orlando, Florida

SIMULATION OF DIRECT CONTACT CONDENSATION OF STEAM JETS SUBMERGED IN SUBCOOLED WATER BY MEANS OF A ONE-DIMENSIONAL TWO-FLUID MODEL

Heinze D.[a,b,*], Schulenberg T.[b] and Behnke L.[a]

[a] Mechanical Engineering,
Kernkraftwerk Gundremmingen GmbH,
Dr.-August-Weckesser-Str. 1,
89355 Gundremmingen,
Germany

[b] Institute for Nuclear and Energy Technologies,
Karlsruhe Institute of Technology,
Hermann-von-Helmholtz-Platz 1,
76344 Eggenstein-Leopoldshafen,
Germany

[*] Author for correspondence
E-mail: david.heinze@partner.kit.edu

ABSTRACT

A one-dimensional simulation model for the direct contact condensation of steam in subcooled water is presented. The model allows to determine major parameters of the process such as the jet penetration length and the axial development of the temperature. Entrainment of water by the steam jet is modeled according to the turbulent entrainment assumption, which can be derived from the Kelvin-Helmholtz instability theory. The steam-water two-phase flow obtained during the mixing process is simulated based on a one-dimensional two-fluid model. An interfacial area transport equation is used to track changes of the interfacial area density due to droplet entrainment and steam condensation. Interfacial heat and mass transfer rates during condensation are calculated using the two-resistance model. The resulting two-phase flow equations constitute a system of ordinary differential equations which is discretized by means of an explicit Runge-Kutta method. The model shows good agreement with published data of pool direct contact condensation experiments at low steam mass flux.

INTRODUCTION

The direct contact condensation (DCC) of a high-velocity steam jet in subcooled water offers a highly efficient means of steam condensation and is therefore used in many industrial applications, such as thermal degasification, direct contact heat exchangers or the depressurization systems of current light water reactors. Furthermore, the phenomenon is of particular importance for the operation of steam-driven jet pumps, where efficient steam condensation is crucial for stable operation.

The DCC process can be divided into two parts. First, the interface between the steam jet and the water pool is disrupted due to the high velocity difference between the two phases. The large interfacial area density obtained by this turbulent mixing process then establishes the basis for rapid steam condensation with heat transfer coefficients up to 10^6 W/(m^2 K). Accordingly, the initial development of the two-phase flow is mainly governed by the momentum transfer from the high-velocity steam to the entrained droplets, while mass and heat transfer dominate with growing interfacial area density.

PREVIOUS WORK

Numerous experimental and theoretical studies of direct contact condensation have been performed in the past to gain a better understanding of the occurring physical phenomena. However, experimental data is mostly limited to the global flow structure. Reliable information regarding the local fluid-dynamic properties is limited due to the complex two-phase flow which impedes experimental measurements.

Experimental observations

In general, three different DCC condensation modes can be distinguished: chugging, bubbling and jetting [1]. The oscillating flow modes of chugging and bubbling occur at low steam mass fluxes, while a stable jet flow appears as soon as the steam flow is choked, i. e. for sonic or supersonic steam injection [2]. The present paper focuses on the stable jetting regime.

Three flow regimes have been observed during stable jet condensation [2]–[4]. First, a vapor core (also called steam cavity) in the immediate proximity of the injection nozzle, where the flow velocity is almost constant [5]. This region is followed by the mixing region, where liquid droplets are entrained into the vapor core and provide a large interfacial area for steam condensation. The third region is the condensation-induced turbulent liquid jet, which has been shown to be in good agreement with turbulent jet

NOMENCLATURE

a_{if}	[m^2/m^3]	interfacial area density
B	[−]	condensation driving potential
c	[m/s]	velocity
c_p	[J/(kg K)]	specific heat capacity at constant pressure
d	[m]	diameter
E_0	[−]	entrainment coefficient
h	[J/kg]	specific enthalpy
h_{lg}	[J/kg]	specific condensation enthalpy
L	[−]	dimensionless jet penetration length
l	[m]	jet penetration length
La	[−]	Laplace number
Ma	[−]	Mach number
$\dot{m}$	[kg/(m^2 s)]	mass flux
$\dot{n}$	[1/(m^2 s)]	particle flux
Nu	[−]	Nusselt number
p	[Pa]	pressure
Pr	[−]	Prandtl number
q	[W/m^2]	heat flux
R	[m]	jet radius
Re	[−]	Reynolds number
S_m	[−]	transport modulus
T	[K]	temperature
We	[−]	Weber number
z	[m]	axial distance

Special characters

α	[W/(m^2 K)]	heat transfer coefficient
ε	[−]	volume fraction
η	[kg/(m s)]	dynamic viscosity
Γ	[kg/(m^3 s)]	volumetric mass source term
λ	[W/(m K)]	thermal conductivity
Φ	[1/(m s)]	interfacial area source term
ρ	[kg/m^3]	density
σ	[kg/s^2]	surface tension

Subscripts

$*$	critical value
0	stagnation condition
∞	ambient property
20	surface-averaged mean value
30	volume-averaged mean value
32	Sauter-averaged mean value
c	continuous phase
d	dispersed phase
crit	critical condition (at sonic velocity)
en	entrainment
e	nozzle exit condition
g	gas phase
if	interface property
l	liquid phase
m	jet mixture property
max	maximum value
sat	saturation

theory [5], [6].

Gas dynamic effects, namely oblique shocks and expansion waves have been observed in over- and under-expanded jets [7], [8]. These phenomena influence the flow structure near the nozzle exit and become more pronounced with increasing water temperature.

One of the major parameters to characterize the DCC flow is the dimensionless jet penetration length L, which is defined as the ratio of the jet penetration length l [m] and the nozzle exit diameter d_e [m]:

$$L = l/d_e \tag{1}$$

Most measurements of L rely on visual observation and are therefore subject to a large experimental bias [9]. Nevertheless, various investigators have shown that L is mainly dependent on the steam mass flux and the temperature of the water pool [3].

Modeling approaches

Kerney *et al.* [10] derived a semi-empirical correlation for the jet penetration length based on the nozzle diameter, the steam mass flux at the nozzle exit $\dot{m}_e$ [kg/(m^2 s)] and the rate of subcooling:

$$L = l/d_e = S_m \left(\frac{\dot{m}_e}{\dot{m}_{crit}} \right)^{0.5} B^{-1} \tag{2}$$

Here, the transport modulus S_m is an empirical parameter analogous to the Stanton number of convective heat transfer, and $\dot{m}_{crit}$ is the critical steam mass flux at ambient water pressure. The condensation driving potential B is defined as

$$B = \frac{c_p \left(T_{sat} - T_\infty \right)}{h_{lg}} \quad , \tag{3}$$

where c_p is the specific heat capacity at constant pressure [J/(kg K)], T_{sat} and T_∞ are the saturation temperature [K] and the temperature of the ambient water, respectively, and h_{lg} is the specific condensation enthalpy [J/kg].

This correlation was later revised [11] based on a single-fluid model in order to account for the influence of water pressure, droplet entrainment and bubble formation. Nevertheless, most subsequent authors have relied on the original formulation when deriving similar correlations [4], [6]–[8], [12].

In general, these empirical correlations agree well with the experimental data that was used to derive the correlation. However, there is substantial disagreement when applying the various correlations to a single experimental data set [9].

More detailed analyses have been performed using computational fluid dynamics (CFD). In most models, the void distribution and the rate of condensation are estimated based on local turbulence values [9], often in conjunction with a probability density function [13]. Additional information can be found in a review article by Gulawani *et al.* [14].

In summary, it can be said that the available empirical correlations on the one hand are limited in their range of applicability. On the other hand, CFD models offer a better modeling accuracy, but at a high computational cost. Therefore, the object of the present work is the development of a one-dimensional simulation model which accounts for the dominant physical processes (entrainment of water droplets into the jet core, formation of a steam-water interface, condensation of steam) and which is capable of predicting major jet parameters such as the jet penetration length and the axial development of the temperature.

DIRECT CONTACT CONDENSATION MODEL

Theoretical model

Immediately after steam injection, the jet consists of a conical vapor core surrounded by the pool water, similar to annular two-phase flow. However, the flow is by no means fully developed: Initially, there is a sharp radial velocity gradient at the boundary between the vapor core and the surrounding stagnant water. Waves are formed at this boundary and liquid ligaments are entrained into the gas core, rapidly breaking up into small droplets. These droplets will cause a quick deceleration of the gas phase due to their high inertia. Accordingly, the radial velocity profile

will flatten with increasing distance from the nozzle. At the same time, steam condenses upon the entrained droplets and the volume fraction ε decreases, finally resulting in a dispersed bubbly flow with negligible slip.

There exists little experimental data regarding the local flow structure of a turbulent condensing two-phase jet. Therefore, some simplifying assumptions have been made in the model development where necessary, in particular regarding the jet profile and the changes in the flow regime. In contrast, appropriate physical model accuracy has been sought regarding the dominant processes of water entrainment and steam condensation.

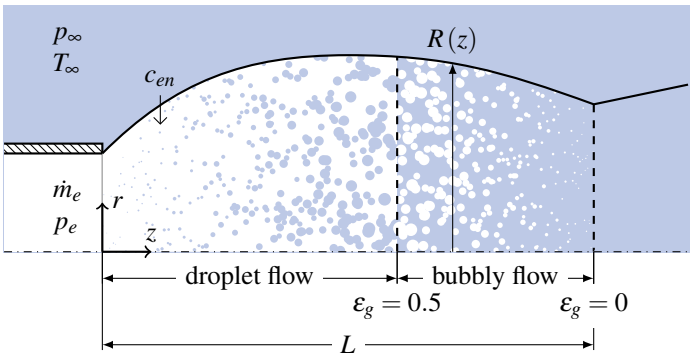

Figure 1 The DCC flow model divides the two-phase jet into a dispersed droplet flow regime and a dispersed bubbly flow regime which are surrounded by the stagnant water.

As can been seen from Figure 1, the model divides the jet region into two areas: The two-phase jet and the surrounding, stagnant water. The two-phase jet flow is initially considered as a dispersed droplet flow, which turns into a dispersed bubbly flow at $\varepsilon = 0.5$.

Mass entrainment from the water pool into the jet is considered to be the dominant exchange mechanism, therefore heat conduction and momentum transfer due to interfacial shear are neglected. Entrainment is modeled according to the turbulent entrainment assumption (explained in detail below), and is assumed to be perpendicular to the flow axis. Accordingly, the entrained mass is added to the two-phase jet without momentum in the axial direction. In the droplet flow regime, the diameter of entrained droplets is obtained based on the initial velocity difference between the entrained droplet and the jet.

In the two-phase jet, no slip has been assumed between the dispersed and the continuous phase. This assumption holds that entrained mass is immediately accelerated to the jet velocity.

Conservation equations

The conservation equations for the two-phase jet are derived under the following assumptions: The flow is stationary, one-dimensional and in mechanical equilibrium (no slip). Gravity, dissipation, shear stresses and heat conduction are neglected. Due to the high density difference between gas and liquid phase at ambient pressure, the kinetic energy of the vapor is small with respect to the inertia of the entrained water. Accordingly, kinetic energy is neglected with respect to enthalpy. The pressure p is assumed to be constant and equal to the pool pressure p_∞, while the jet radius R is a function of the axial distance z.

Then, the mass conservation equations for the gas phase g and the liquid phase l have the form

$$\frac{\mathrm{d}}{\mathrm{d}z}\left(\varepsilon_g \rho_g c_z R^2\right) = \Gamma_g R^2 \quad , \tag{4}$$

$$\frac{\mathrm{d}}{\mathrm{d}z}\left(\varepsilon_l \rho_l c_z R^2\right) = \left(\Gamma_l + \Gamma_{en,l}\right) R^2 \quad , \tag{5}$$

where ρ is the density [kg/m^3], c_z is the axial velocity, $\Gamma_{en,l}$ is the volumetric mass source term [kg/(m^3 s)] due to entrainment, and Γ_g and Γ_l are the volumetric mass source terms due to phase change in the gas and the liquid phase, respectively.

Introducing the mixture density ρ_m as

$$\rho_m = \varepsilon_g \rho_g + \varepsilon_l \rho_l \quad , \tag{6}$$

the mixture momentum equation can be written as

$$\frac{\mathrm{d}}{\mathrm{d}z}\left(\rho_m c_z^2 R^2\right) = 0 \quad . \tag{7}$$

The energy conservation for the gas and the liquid phase are written as

$$\frac{\mathrm{d}}{\mathrm{d}z}\left(\varepsilon_g \rho_g c_z h_g R^2\right) = \left(\Gamma_g h_{g,if} + a_{if} q_{g,if}\right) R^2 \quad , \tag{8}$$

$$\frac{\mathrm{d}}{\mathrm{d}z}\left(\varepsilon_l \rho_l c_z h_l R^2\right) = \left(\Gamma_l h_{l,if} + \Gamma_{en,l} h_\infty + a_{if} q_{l,if}\right) R^2 \quad , \tag{9}$$

where h_g and h_l are the gas and liquid phase enthalpy [J/kg], respectively, $h_{g,if}$ and $h_{l,if}$ are the enthalpies on the gas and liquid side of the phase interface, respectively, h_∞ is the ambient water enthalpy, a_{if} is the interfacial area density [m^2/m^3], and $q_{g,if}$ and $q_{l,if}$ represent the heat flux [W/m^2] on the gas and the liquid side of the interface, respectively.

The interfacial transfer conditions are given by

$$\Gamma_g + \Gamma_l = 0 \quad , \tag{10}$$

$$\Gamma_g h_{g,if} + a_{if} q_{g,if} + \Gamma_l h_{l,if} + a_{if} q_{l,if} = 0 \quad , \tag{11}$$

and the enthalpies on the interface $h_{g,if}$ and $h_{l,if}$ are assumed to be equal to the gas and liquid saturation enthalpies.

Interfacial area transport

In addition to the conservation equations, an interfacial area transport equation [15] for the dispersed phase d is used to track the change of the interfacial area density a_{if} due to droplet entrainment, droplet growth and bubble condensation:

$$\frac{\mathrm{d}}{\mathrm{d}z}\left(a_{if} c_d R^2\right) = \left(\Phi_{en} + \frac{2}{3}\frac{a_{if}}{\rho_d}\left(\frac{\Gamma_d}{\varepsilon_d} - c_d \frac{\mathrm{d}\rho_d}{\mathrm{d}z}\right)\right) R^2 \tag{12}$$

Here, the interfacial area source term due to droplet entrainment Φ_{en} [1/(m s)] is calculated as

$$\Phi_{en} = \frac{2}{R}\dot{n}_{en}\pi d_{20,en}^2 \quad , \tag{13}$$

with the particle flux $\dot{n}$ [1/(m^2 s)] of entrained droplets across the jet boundary

$$\dot{n}_{en} = \frac{6}{\pi} \frac{c_{en}}{d_{30,en}^3} \quad . \tag{14}$$

In equations (13) and (14), d_{20} and d_{30} are the surface and volume mean diameters, respectively. Combining equations (13) and (14) and introducing the Sauter mean diameter $d_{32} = d_{30}^3/d_{20}^2$ yields

$$\Phi_{en} = \frac{12}{R} \frac{c_{en}}{d_{32,en}} \quad . \tag{15}$$

Turbulent entrainment

The mixing of two miscible fluids flowing with different velocities can be described by the turbulent entrainment assumption, initially derived for hot gases rising in air [16], [17]. The theory has been extended to miscible gases with high density differences [18], resulting in the following equation for the entrainment velocity c_{en}:

$$c_{en} = E_0 \sqrt{\frac{\rho_m}{\rho_\infty}} c \tag{16}$$

Here, ρ_∞ is the density of the entrained fluid and ρ_m is the local mean density of a jet flowing with the velocity c. The empirical entrainment coefficient E_0 has been experimentally determined in the range of 0.06 to 0.12 with a recommended value of 0.08.

Equation (16) has been successfully applied to gas and vapor jets in subcooled liquids [11], [19]. This extension from miscible to immiscible fluids can be corroborated using the Kelvin-Helmholtz instability theory [20]. Here, fluid entrainment is described by the formation of a capillary wave at the phase boundary which breaks up into a ridge of liquid, yielding the following relationship for the entrainment velocity:

$$c_{en} \sim \sqrt{\frac{\rho_m}{\rho_\infty}} \frac{\rho_\infty}{\rho_\infty + \rho_m} c \tag{17}$$

Equation (17) reduces to equation (16) for $\rho_\infty \gg \rho_m$ and a proportionality constant E_0.

Using equation (17) with an appropriate entrainment coefficient allows to calculate the volumetric mass source term due to entrainment:

$$\Gamma_{en,l} = \frac{2}{R} \rho_\infty c_{en} \quad . \tag{18}$$

Size of entrained droplets

In the droplet flow regime, the entrained liquid ligaments will break up under the impact of the aerodynamic drag force due to the jet velocity. The maximum diameter of entrained droplets $d_{max,en}$ can be determined implicitly as a function of the critical Weber number We^* [21]:

$$d_{max,en} = \frac{We^*\left(d_{max,en}\right) \sigma}{\rho_m \left(c_z - c_\infty\right)^2} \tag{19}$$

$$We^*\left(d_{max,en}\right) = 12 \left(1 + 1.5 \cdot La_{d,en}^{-0,37}\right) \tag{20}$$

$$La_{d,en} = \frac{\rho_\infty \sigma d_{max,en}}{\eta_\infty^2} \tag{21}$$

In equations (19) to (21), σ is the surface tension [kg/s^2] of the droplet, c_∞ is the axial droplet velocity immediately after entrainment (assumed to be zero as described above), $La_{d,en}$ is the Laplace number of a droplet having the maximum stable diameter and η_∞ is the droplet dynamic viscosity [kg/(m s)].

Assuming an upper log-normal size distribution, the ratios between the surface, volume and Sauter mean diameters (d_{20}, d_{30}, d_{32}) and the maximum droplet diameter are taken as [21], [22]

$$\frac{d_{20}}{d_{max}} = 0.11 \ , \quad \frac{d_{30}}{d_{max}} = 0.14 \ , \quad \frac{d_{32}}{d_{max}} = 0.25 \quad . \tag{22}$$

Interfacial heat and mass transfer

Interfacial heat and mass transfer has been modeled with the two-resistance model for the phase change in pure substances. This approach considers the heat transfer processes on each side of the phase interface, where the heat flux q can be written as

$$q_{l,if} = \alpha_l \left(T_{sat} - T_l\right) + \dot{m}_{g\to l} h_{l,if} \quad , \tag{23}$$

$$q_{g,if} = \alpha_g \left(T_{sat} - T_g\right) - \dot{m}_{g\to l} h_{g,if} \quad . \tag{24}$$

Here, α is the heat transfer coefficient [W/(m^2 K)] and $\dot{m}_{g\to l}$ is the mass flux from the gas to the liquid phase.

Then, the mass flux can be determined from the heat flux balance ($q_l + q_g = 0$) as

$$\dot{m}_{g\to l} = \frac{\alpha_l \left(T_{sat} - T_l\right) + \alpha_g \left(T_{sat} - T_g\right)}{h_{g,if} - h_{l,if}} \quad . \tag{25}$$

In the bubbly flow regime, the heat transfer coefficient across interface and the dispersed phase α_d is set to $\alpha_g = 10^4$ W/(m^2 K) [24]. In effect, the bubble temperature will quickly approach the interface temperature T_{sat}. Due to the small size of the entrained droplets, the same approach can be used to model the heat transfer in the dispersed droplet regime, thus:

$$\alpha_d = 10^4 \frac{\mathrm{W}}{\mathrm{m^2\,K}} \tag{26}$$

The heat transfer coefficient in the continuous phase α_c (α_g in the droplet flow regime, α_l in the bubbly flow regime) is determined based on the Nusselt number Nu:

$$\alpha_c = \frac{\lambda_c Nu_c}{d_d} \tag{27}$$

The Nusselt number for $0 \le Pr_c \le 250$ is calculated according to Hughmark [25]:

$$Nu_c = \begin{cases} 2 + 0.6 Re_{dc}^{0.5} Pr_c^{0.33} & ; \quad 0 \le Re_{dc} < 776.06 \\ 2 + 0.27 Re_{dc}^{0.62} Pr_c^{0.33} & ; \quad 776.06 \le Re_{dc} \end{cases} \tag{28}$$

In equation (28), the relative Reynolds number between the dispersed and the continuous phase Re_{dc} and the Prandtl number of the continuous phase Pr_c are defined as

$$Re_{dc} = \frac{\rho_c |c_d - c_c| d_d}{\eta_c} \quad , \tag{29}$$

Title	Stagnation pressure	Nozzle throat		Nozzle exit		Ref.
		diameter	mass flux	diameter	mass flux	
	p_0/bar	d_{crit}/mm	$\dot{m}_{crit}$/kg/(m^2 s)	d_e/mm	$\dot{m}_e$/kg/(m^2 s)	
WU07A-2	2	2.0	298	2.2		[23]
WU07A-4	4	2.0	441	2.2		[23]
WU07B-2	2	2.0	298	3.0		[23]
WU07B-4	4	2.0	441	3.0		[23]
WU10-3	3	8.0		11.2	225	[4]
WU10-5	5	8.0		11.2	370	[4]

Table 1 Parameters of selected DCC experiments taken from the literature. All experiments have been performed at ambient pool conditions ($p_\infty \approx 1$ bar).

$$Pr_c = c_p \eta_c / \lambda_c \quad . \tag{30}$$

Therefore, equation (28) reduces to $Nu_c = 2$ when no phase slip is assumed ($c_d = c_c$).

Finally, the volumetric mass source term can be obtained as

$$\Gamma_l = a_{if} \cdot \dot{m}_{g \to l} \quad . \tag{31}$$

Simulation model

The conservation equations (4), (5) and (7) to (9) and the interfacial transport equation (12) constitute a system of six ordinary differential equations for the variables R, c_z, ε, h_g, h_l and a_{if}. The system is solved using an explicit fourth-order Runge-Kutta algorithm.

Gas-dynamic phenomena due to over- and under-expansion are neglected and the effective-adapted-jet approximation is applied as boundary condition at the nozzle exit. This approach is widely used in treating two-phase jets with and without condensation [26] and assumes isentropic adaptation to the ambient water pressure p_∞. The nozzle exit velocity, density and diameter are then replaced by the adapted values. Additionally, a maximum void fraction of $\varepsilon_g = 1 - 10^{-8}$ is enforced at the nozzle exit to avoid numerical errors due to division by zero.

Subsequently, each solver step consists of the following major sub-steps:

1. Thermodynamic properties are calculated using the IAPWS-IF97 equation of state [27] as a function of the pool pressure p_∞ and the gas and liquid phase enthalpies h_g and h_l.
2. The entrainment velocity c_{en} and volumetric mass source term $\Gamma_{en,l}$ are calculated using equations (17) and (18) with an entrainment coefficient of $E_0 = 0.08$.
3. Equations (19) to (21) are iteratively solved to obtain the maximum diameter of entrained droplets $d_{max,en}$, which is then used to calculate the Sauter mean diameter $d_{32,en}$ and the interfacial area source term due to droplet entrainment Φ_{en} according to equation (22) and equation (15), respectively.
4. Interfacial heat and mass transfer ($q_{g,if}$, $q_{l,if}$, $\dot{m}_{g \to l}$, Γ_l) is solved using equations (23) to (31).
5. The conservation equations and the interfacial transport equation (equations (4), (5), (7) to (9) and (12)) are solved using the explicit Runge-Kutta-Fehlberg algorithm.

Initially, the solver is invoked for dispersed droplet flow (liquid phase l = dispersed phase d). The solver proceeds until $\varepsilon_g = 0.5$ is reached, where the solver is re-initialized for dispersed bubbly flow (gas phase g = dispersed phase d) and continues until a minimum void fraction of $\varepsilon_g = 10^{-6}$ is reached. The axial distance at this point corresponds to the predicted penetration length: $z\left(\varepsilon_g = 10^{-6}\right) = l$.

SIMULATION RESULTS

The simulation model has been compared to various experiments taken from the literature, which cover a wide range of parameters (nozzle exit diameter, mass flux and pressure, pool water temperature). Details on the selected experiments are given in Table 1.

The stagnation state has been determined using the stagnation pressure p_0 provided in the literature while assuming a saturated steam state. Non-equilibrium effects during expansion (cf. [28]) have been neglected, as not all literature sources provided sufficient information about the nozzle geometry. Accordingly, the nozzle exit state has been determined assuming isentropic equilibrium expansion. The simulated nozzle exit conditions obtained in this manner are given in Table 2 and are in good agreement with the experimental data.

Jet penetration length

In Figures 2a and 2b, the simulated dimensionless jet penetration length L for different nozzle exit conditons and pool temperatures is compared with the experimental measurements from [4], [23]. Figure 2a shows the results for low stagnation pressures and accordingly low steam mass fluxes. Here, the simulation is in good agreement with the experimental data. However, L is underpredicted for higher mass fluxes, as can be seen in Figure 2b.

Axial temperature profile

In addition to the jet penetration length, the axial temperature profile of the two-phase jet has been measured in [4]. However, it was not possible to determine whether this data should

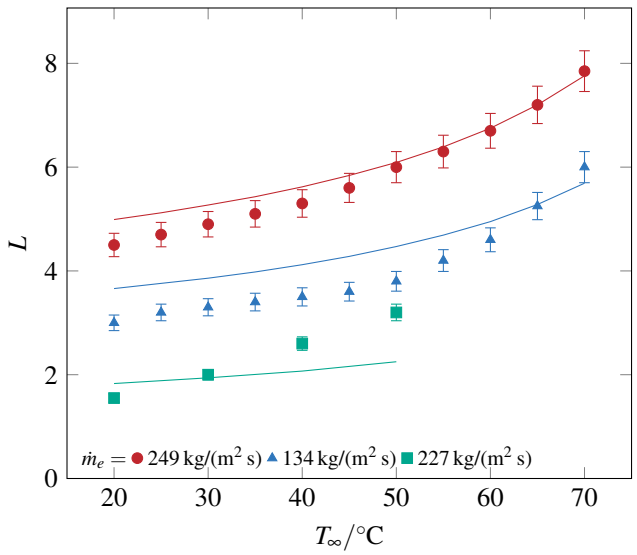

(a) Low steam mass flux: Experimental values (● WU07A-2; ▲ WU07B-2; ■ WU10-3) and respective simulation results (——; ——; ——).

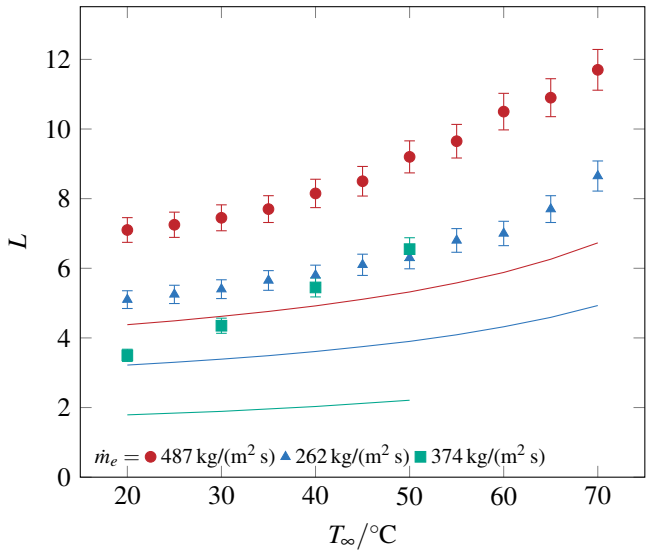

(b) High steam mass flux: Experimental values (● WU07A-4; ▲ WU07B-4; ■ WU10-5) and respective simulation results (——; ——; ——).

Figure 2 Dimensionless penetration length L for different pool temperatures T_∞.

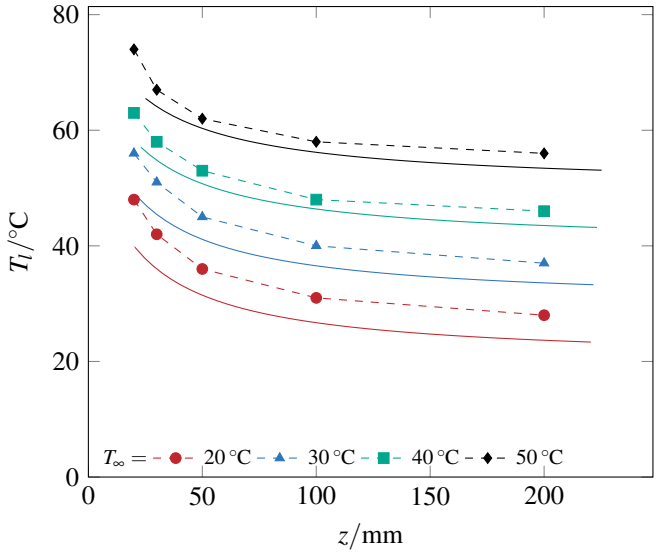

(a) Experiment WU10-3 ($\dot{m}_e = 227.410\,\mathrm{kg/(m^2\,s)}$)

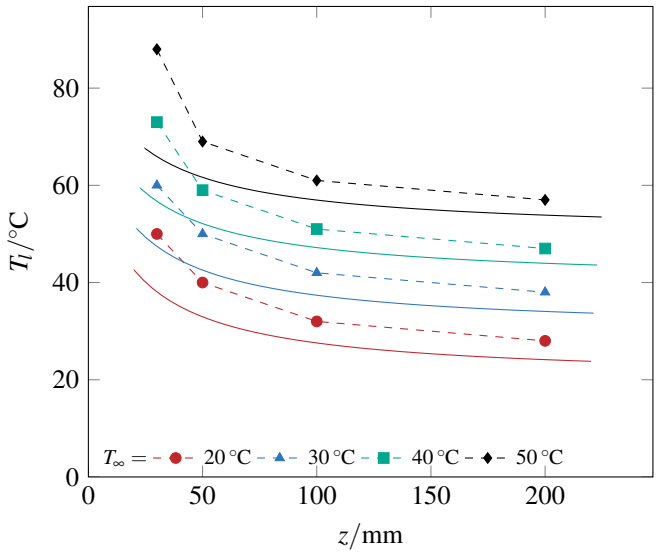

(b) Experiment WU10-5 ($\dot{m}_e = 373.531\,\mathrm{kg/(m^2\,s)}$)

Figure 3 Temperature profile T_l along the jet axis z for the condensation-induced single phase jet: Experimental values for different pool temperatures T_∞ (● 20 °C; ▲ 30 °C; ■ 40 °C; ♦ 50 °C) and respective simulation results (——; ——; ——; ——).

Title	Nozzle exit			
	Mach number Ma_e	mass flux $\dot{m}_e$/kg/(m^2 s)		pressure p_e/bar
WU07A-2	1.4	248.5	(0.9 %)	0.6
WU07A-4	1.4	487.1	(1.1 %)	1.2
WU07B-2	1.9	133.6	(0.9 %)	0.2
WU07B-4	2.0	262.0	(1.1 %)	0.4
WU10-3	1.8	227.4	(1.1 %)	0.4
WU10-5	1.9	373.5	(1.0 %)	0.7

Table 2 Simulation results for the flow conditions at the nozzle exit. Values in parentheses indicate the deviation from the literature data.

be correlated to the simulated temperature in the gas or the liquid phase. These difficulties do not arise in the condensation-induced single-phase jet region. Accordingly, comparisons of the axial temperature profile were limited to this region ($z > l$). For this purpose, the simulation was continued from the end of the two-phase flow region by setting $\varepsilon_l = 1$ and $\Gamma_l = q_{l,if} = 0$, which converts equations (5), (7) and (9) into the conservation equations for a single-phase jet with turbulent entrainment.

The results obtained in this manner for the axial temperature profile are shown in Figures 3a and 3b for experiments WU10-3 and WU10-5, respectively. Again, the simulation model is capable of predicting the experimental data at low mass flux, while no adequate agreement could be achieved for the experiments at high mass flux.

Interpretation of results

The jet penetration length is mainly dependent on the water temperature and the steam mass flux. The simulation results regarding the influence of the pool water temperature are in good agreement with experimental data. However, the increase in penetration length when increasing the steam mass flux could not be predicted by the developed model. Therefore, the model underestimates the penetration length of the two-phase jet and the axial temperature profile of the condensation-induced single phase jet at high steam mass fluxes, but matches closely with experimental data for low steam mass fluxes.

The two major physical processes in the two-phase jet region are the mass entrainment at the jet boundary and the condensation in the jet core, while only the former is relevant in the single-phase jet region. Since the simulation data is in good agreement with the experimental data in the single-phase jet region, the entrainment model on the one hand (equations (17) and (18)) is considered to be valid. On the other hand, it is believed that additional research is required to improve the condensation model, particularly with respect to the calculation of the interfacial area density.

CONCLUSION

In the present work, turbulent entrainment and the development of the interfacial area density are considered to be the dominant processes during direct contact condensation of a steam jet in subcooled water. Accordingly, it has been attempted to model these phenomena in a physically sound manner, while applying appropriate simplifications regarding the development of the jet profile and the changes in the flow regime.

The simulation results are in good qualitative agreement with experimental data, supporting the validity of the modeling approach. Quantitative accordance is achieved for steam injection at low mass fluxes. It is believed that a more detailed modeling of the interfacial area density will improve the simulation accuracy at higher steam mass fluxes.

ACKNOWLEDGEMENTS

This work is financially supported by the RWE Power AG.

REFERENCES

[1] C. Chan and C. Lee, "A regime map for direct contact condensation", *International Journal of Multiphase Flow*, vol. 8, no. 1, pp. 11–20, Feb. 1982.

[2] C. H. Song and Y. S. Kim, "Direct contact condensation of steam jet in a pool", *Advances in Heat Transfer*, vol. 43, p. 227, 2011.

[3] C.-H. Song, S. Cho, and H.-S. Kang, "Steam jet condensation in a pool: from fundamental understanding to engineering scale analysis", *Journal of Heat Transfer*, vol. 134, no. 3, pp. 031 004–1 –031004–15, 2012.

[4] X.-Z. Wu, J.-J. Yan, W.-J. Li, D.-D. Pan, and G.-Y. Liu, "Experimental investigation of over-expanded supersonic steam jet submerged in quiescent water", *Experimental Thermal and Fluid Science*, vol. 34, no. 1, pp. 10–19, 2010.

[5] S. K. Dahikar, M. J. Sathe, and J. B. Joshi, "Investigation of flow and temperature patterns in direct contact condensation using PIV, PLIF and CFD", *Chemical Engineering Science*, vol. 65, no. 16, pp. 4606–4620, Aug. 2010.

[6] X.-Z. Wu, J.-J. Yan, W.-J. Li, D.-D. Pan, and G.-Y. Liu, "Experimental study on a steam-driven turbulent jet in subcooled water", *Nuclear Engineering and Design*, vol. 240, no. 10, pp. 3259–3266, 2010.

[7] H. Y. Kim, Y. Y. Bae, C. H. Song, J. K. Park, and S. M. Choi, "Experimental study on stable steam condensation in a quenching tank", *International Journal of Energy Research*, vol. 25, no. 3, 239–252, 2001.

[8] X.-Z. Wu, J.-J. Yan, S.-F. Shao, Y. Cao, and J.-P. Liu, "Experimental study on the condensation of supersonic steam jet submerged in quiescent subcooled water: steam plume shape and heat transfer", *International Journal of Multiphase Flow*, vol. 33, no. 12, pp. 1296–1307, 2007.

[9] S. S. Gulawani, J. B. Joshi, M. S. Shah, C. S. RamaPrasad, and D. S. Shukla, "CFD analysis of flow pattern and heat transfer in direct contact steam condensation", *Chemical Engineering Science*, vol. 61, no. 16, pp. 5204–5220, 2006.

[10] P. J. Kerney, G. M. Faeth, and D. R. Olson, "Penetration characteristics of a submerged steam jet", *AIChE Journal*, vol. 18, no. 3, 548–553, 1972.

[11] J. C. Weimer, G. M. Faeth, and D. R. Olson, "Penetration of vapor jets submerged in subcooled liquids", *AIChE Journal*, vol. 19, no. 3, 552–558, 1973.

[12] M.-H. Chun, Y.-S. Kim, and J.-W. Park, "An investigation of direct condensation of steam jet in subcooled water", *International Communications in Heat and Mass Transfer*, vol. 23, no. 7, pp. 947–958, 1996.

[13] L.-D. Chen and G. M. Faeth, "Condensation of submerged vapor jets in subcooled liquids", *Journal of Heat Transfer*, vol. 104, no. 4, pp. 774–780, 1982.

[14] S. S. Gulawani, S. S. Deshpande, J. B. Joshi, *et al.*, "Submerged gas jet into a liquid bath: a review", *Industrial & Engineering Chemistry Research*, vol. 46, no. 10, pp. 3188–3218, 2007.

[15] M. Ishii and S. Kim, "Development of one-group and two-group interfacial area transport equation", *Nuclear science and engineering*, vol. 146, no. 3, 257–273, 2004.

[16] G. I. Taylor, "Dynamics of a mass of hot gas rising in air", Los Alamos National Laboratory, Tech. Rep. LA-236, 1945.
[17] B. R. Morton, G. Taylor, and J. S. Turner, "Turbulent gravitational convection from maintained and instantaneous sources", *Proceedings of the Royal Society of London. Series A. Mathematical and Physical Sciences*, vol. 234, no. 1196, pp. 1–23, 1956.
[18] F. P. Ricou and D. B. Spalding, "Measurements of entrainment by axisymmetrical turbulent jets", *Journal of Fluid Mechanics*, vol. 11, no. 1, pp. 21–32, 1961.
[19] H. K. Fauske and M. A. Grolmes, "Mitigation of hazardous emergency release source terms via quench tanks", *Plant/Operations Progress*, vol. 11, no. 2, 121–125, 1992.
[20] M. Epstein and H. Fauske, "Applications of the turbulent entrainment assumption to immiscible gas-liquid and liquid-liquid systems", *Chemical Engineering Research and Design*, vol. 79, no. 4, pp. 453–462, 2001.
[21] V. Alipchenkov, R. Nigmatulin, S. Soloviev, *et al.*, "A three-fluid model of two-phase dispersed-annular flow", *International Journal of Heat and Mass Transfer*, vol. 47, no. 24, pp. 5323–5338, 2004.
[22] B. Azzopardi, "Drops in annular two-phase flow", *International Journal of Multiphase Flow*, vol. 23, no. 7, pp. 1–53, 1997.
[23] X.-Z. Wu, J.-J. Yan, W.-J. Li, D.-D. Pan, and D.-T. Chong, "Experimental study on sonic steam jet condensation in quiescent subcooled water", *Chemical Engineering Science*, vol. 64, no. 23, pp. 5002–5012, 2009.
[24] G. G. Brucker and E. M. Sparrow, "Direct contact condensation of steam bubbles in water at high pressure", *International Journal of Heat and Mass Transfer*, vol. 20, no. 4, pp. 371–381, 1977.
[25] G. A. Hughmark, "Mass and heat transfer from rigid spheres", *AIChE Journal*, vol. 13, no. 6, 1219–1221, 1967.
[26] E. Loth and G. Faeth, "Structure of underexpanded round air jets submerged in water", *International Journal of Multiphase Flow*, vol. 15, no. 4, pp. 589–603, 1989.
[27] W. Wagner, J. R. Cooper, A. Dittmann, *et al.*, "The IAPWS industrial formulation 1997 for the thermodynamic properties of water and steam", *Journal of Engineering for Gas Turbines and Power*, vol. 122, no. 1, pp. 150–185, 2000.
[28] D. Heinze, T. Schulenberg, and L. Behnke, "Modeling of steam expansion in a steam injector by means of the classical nucleation theory", in *Proceedings of The 15th International Topical Meeting on Nuclear Reactor Thermal Hydraulics (NURETH-15)*, Pisa, 2013.